A structural transformation and its effect on the physical properties of the V-substituted $Bi_2Sr_2Ca_2Cu_3O_{10+y}$ system

1997 J. Phys.: Condens. Matter 9 1105

(http://iopscience.iop.org/0953-8984/9/5/015)

J. Phys.: Condens. Matter **9** (1997) 1105–1121. Printed in the UK PII: S0953-8984(97)72959-X

A structural transformation and its effect on the physical properties of the V-substituted $Bi_2Sr_2Ca_2Cu_3O_{10+y}$ system

M E Yakıncı

İnönü Üniversitesi, Fen Edebiyat Fakültesi, Fizik Bölümü, 44069 Malatya, Turkey

Received 20 March 1996, in final form 30 August 1996

Abstract. Systematic substitution of V in the $Bi_{2-\delta}V_\delta Sr_2Ca_2Cu_3O_{10+y}$ system ($\delta = 0$, 0.2, 0.4, 0.6, 0.8 and 1) was carried out in order to determine the effect of V ions on the phase formation and on the physical properties of the BSCCO 2223 system. The most interesting observation was structural transformation of the system from tetragonal to orthorhombic after $\delta = 0.6$. A solid solubility limit for V was also found to exist. Resistivity and susceptibility studies have shown that high-T_c superconductivity exists up to $\delta = 0.6$ and that the semiconducting-to-metallic transition or fully semiconducting behaviour occurs after this limit. A fractionally small but very-high-T_c transition at around 210 K was also observed, but it was not reproducible. Among the V-substituted samples the best electrical properties were obtained for $\delta = 0.2$; T_c and T_0 were found to be 112 K and 92 K, respectively, the calculated value of J_c was found to be 1.11×10^5 A cm^2 at 4.5 K and the thermal conductivity parameter κ was found to be 6.4 mW cm^{-1} K^{-1}. By substituting the higher-valence state V^{5+} ions for Bi^{3+}, the thermal treatment time is significantly reduced. The magnetic properties, IR and thermal conductivity results showed evidence of a strong coupling mechanism in the $Bi_{2-\delta}V_\delta Sr_2Ca_2Cu_3O_{10+y}$ system.

1. Introduction

Since the discovery that the Bi–Sr–Ca–Cu–O (BSCCO) system [1], mainly contains three phases under the general formula $Bi_2Sr_2Ca_{n-1}Cu_nO_{2n+4+y}$ where $n = 1$, 2 and 3 refer to the number of Cu–O layers and incorporate the 10, 95 and 110 K superconductor phases, respectively [2–4], many studies have been reported about the effect of different dopants or substitutions with different-valence states to clarify whether any improvement is possible in T_c or not [5–15].

In recent years, some interesting results have been obtained for the doping or substitution effects of particularly Ag^{2+}, Pb^{2+}, Tl^{3+}, Sb^{3+}, Mo^{6+} and other ternary oxides on Bi^{3+} sites [16–20]. The results obtained showed that the role of these particular elements is high-T_c phase stabilizers. These elements possibly increase the activation energy of the ions, providing good solid solubility, and accelerate the reaction kinetics which then result in a higher volume fraction of the high-T_c phase. Experiments have also demonstrated that there exist no significant changes in the structural parameters, but most significant changes occur in the carrier concentration because of different cation doping levels [14, 21–23]. Instead of Bi^{3+}, making a substitution to other sites, e.g. to Ca^{3+}, Cu^{2+} or Sr^{2+}, was also investigated and the results obtained showed a transformation from the metallic state to the Mott–Hubbard insulating state. The results obtained indicate the important fact that the rare earths are not always the right choice for enhancement or stabilization of the high-T_c phase in the BSCCO system.

0953-8984/97/051105+17$19.50

Recently some findings on V substitution for different phases of the BSCCO system have been reported: Xin *et al* [24, 25] have worked on the optimum fabrication process; Liu *et al* [26] have investigated Tl–V combinations for the complete replacement of Bi; Fung *et al* [27, 28] have worked on the preparation route and some physical properties such as band structure using the EEM theory and dislocation networks; Chanda *et al* [29] have found evidence of strong electron–phonon coupling; Yakıncı*et al* [30] have produced a glass-ceramic from of V-substituted BSCCO material.

However, none of the above reported the occurrence of any significant transformation in the crystal structure or any possible effect on this transformation on the physical properties. Thus, in this study, the higher-valence state V^{5+} is substituted for Bi^{3+} with various stoichiometries and for the first time the IR-active phonon modes, the structural transformation and the related resistivity results, together with the magnetization data and the thermal conductivity characteristic of each phases are presented.

2. Experimental details

For the initial materials, high-purity (99.99%) powders of Bi_2O_3, V_2O_5, $SrCO_3$, $CaCO_3$ and CuO were used to prepare a nominal composition $Bi_{2-\delta}V_\delta Sr_2Ca_2Cu_3O_{10+y}$, where $\delta = 0$, 0.2, 0.4, 0.6, 0.8 and 1.0. All samples were synthesized using the two-step solid state reaction technique. In the first stage, powders of Bi_2O_3, $SrCO_3$, $CaCO_3$ and CuO were mixed and first calcined at 750 °C for 24 h in air, and then the calcination stage was repeated twice at 820 °C for 24 h with intermediate grinding. In the second stage, V_2O_5 was added to complete the nominal compositions. V mixed precursors were pressed into pellets of diameter 10 mm and of length 2 mm. Each pellet was sealed in an evacuated quartz ampoule and then sintered under different temperature–time combinations. Some of the samples were annealed in an O_2 pressure or in an air atmosphere at 600 °C after having been sealed off from the evacuation in the quartz ampoules; others were either quenched to the room temperature or furnace cooled in the ampoules (table 1).

The crystal structures of the materials were investigated by x-ray diffraction (XRD) analysis using the Rigaku RadB powder diffractometer system and CuKα radiation. All samples were examined with a scan speed of 1° min^{-1} and 2θ between 3 and 65° at room temperature.

The infrared (IR) absorption properties of the samples were investigated using a Fourier transform IR spectrophotometer (Bomem MB100). The IR spectra of pelletized mixture of the KBr and fine powder of samples (1 wt%) were taken between 390 and 1000 cm^{-1} with a spectral resolution of 1 cm^{-1} against a KBr reference at room temperature.

The microstructure and compositional characterizations were carried our with a JEOL JSM-6300 scanning electron microscope and Link System AN10000 energy dispersive x-ray spectroscope.

Resistivity measurements were carried out with a closed-system He refrigerator (Leybold) using the conventional DC four-probe method with a 10 mA constant current. Contacts to the samples were made using conductive silver paint or metallic indium.

The magnetization measurements were carried out using a SQUID magnetometer (Quantum Design model MPMS, 7T) with a magnetic field H parallel to the *c* axis of the sample. The superconductor critical temperature was measured in a zero-field-cooling (ZFC) procedure with an applied field of $\mu_0 H = 10$ G. Then hysteresis cycles were performed at different temperatures and the critical current density was estimated using Bean's model.

The thermal conductivity measurements of materials were made using the steady-state heat flow method between 30 and 200 K. Pellets of diameter 10 mm and of length 1 mm

Table 1. Summary of the preparation conditions and physical properties: Optimum, optimum treatment condition, Q, quenched sample.

	Heating parameters							
Material	Temperature (°C)	Time (h)	Atmosphere	T_c (K)	T_{zero} (K)	ΔT (K)	J_c at 4.5 K (A cm^{-2})	κ (mW cm^{-1} K^{-1})
Optimum $\delta = 0$	845	240	O_2	114	108	6	1.38×10^5	8.6
Optimum $\delta = 0.2$	850	80	O_2	112/97	92	20/5	1.11×10^5	6.4
$\delta = 0.2$	850	80	Air	110/92	86	24/6	1.01×10^5	
$\delta = 0.2$	850	80	Q	90	81	9	0.63×10^5	
Optimum $\delta = 0.4$	850	70	O_2	92	83	9	0.97×10^5	5
$\delta = 0.4$	850	70	Air	89	78	11	0.83×10^5	
$\delta = 0.4$	850	70	Q	86	73	13	0.34×10^5	
Optimum $\delta = 0.6$	845	60	O_2	78	67	11	0.71×10^5	3.3
$\delta = 0.6$	845	60	Air	75	60	15	0.61×10^5	
$\delta = 0.6$	845	60	Q	60	41	19	0.29×10^5	
Optimum $\delta = 0.8$	840	55	O_2	60	30	30	0.34×10^5	
$\delta = 0.8$	840	55	Air	60	30	30	0.33×10^5	
$\delta = 0.8$	840	55	Q	53	22	31	0.14×10^5	
Optimum $\delta = 1.0$	840	40	O_2	15	—	—	—	
$\delta = 1.0$	840	40	Air	—	—	—	—	
$\delta = 1.0$	840	40	Q	—	—	—	—	

were used for the measurements. The bottom end of the specimen was fixed to the cold head of the cryostat system using a conductive silver paint. The upper end of the specimen was attached to a heater (75 Ω) which had an indium sheeted surface. The temperature gradient was monitored using two calibrated Si diodes attached to the ends of the specimens.

3. Results and discussion

3.1. X-ray diffraction investigation

Under the preparation conditions used, it was found that the superconductor high-T_c phase formation largely depended on the heating time, as well as on the heating temperature. In contrast with unsubstituted BSCCO 2223 material (240 h average thermal treatment time necessary for high-T_c phase formation) a short-time heat treatment (55–80 h depending on δ) in V-substituted material actually favours the growth of the high-T_c phase. If the substitution ratio of V^{5+} to Bi^{3+} is increased, then a shorter heating time and a lower temperature is required (table 1).

Figure 1 shows the XRD patterns of the materials prepared with different V-substituted stoichiometries under their optimum treatment conditions. The optimum thermal treatment condition of each stoichiometry was derived by considering the XRD, scanning electron microscopy (SEM)–energy-dispersive x-ray analysis (EDXA), resistivity and magnetization results. For uniformity, structural data have been calculated only for samples heat treated under their optimum conditions using the least-squares fit of the x-ray lines; the microqualitative data obtained from the SEM-EDXA were also taken into account.

In the BSCCO 2223, $\delta = 0$ (unsubstituted) composition, the high-T_c phase developed at 845 °C after a 240 h thermal treatment. Highly c-axis texturing was obtained. This suggests that maximum crystalline nucleation occurred and apparently promoted grain growth along the c-axis (figure 1(a)). The calculated value of the unit-cell parameters showed that

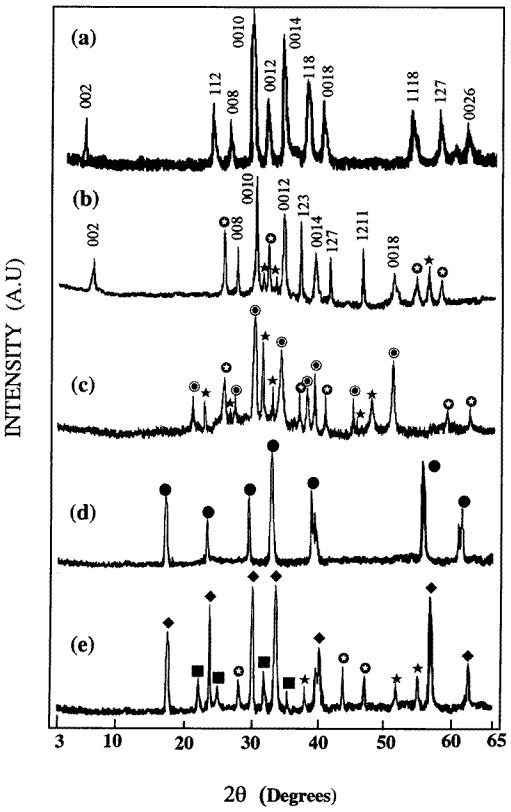

Figure 1. XRD patterns of the $Bi_{2-\delta}V_{\delta}Sr_2Ca_2Cu_3O_{10+y}$ system (Au, arbitrary units). (a) For $\delta = 0$, characteristic peaks of the BSCCO 2223 system obtained after optimum treatment condition. (b) For $\delta = 0.2$, indexed patterns belong to $Bi_{1.77}V_{0.15}Sr_{1.97}Ca_{1.3}Cu_{2.07}O_{8+y}$, $SrVO_3$ (○) and $CaVO_3$ (⋆) phases. (c) For $\delta = 0.4$, $Bi_{1.7}V_{0.31}Sr_{1.96}Ca_{1.11}$ $Cu_{2.05}O_{8+y}$ (◉), $SrVO_3$ (○) and $CaVO_3$ (⋆) phases. (d) For $\delta = 0.6$, $Bi_{1.57}V_{0.48}Sr_{1.94}Ca_{1.10}Cu_{2.00}O_{8+y}$ (●). (e) For $\delta = 0.8$, $Bi_2Sr_2CuO_{6+y}$ (■), $Bi_{1.31}V_{0.54}Sr_{1.85}Ca_{0.92}$ $Cu_{1.96}O_{8+y}$ (⧫), $SrVO_3$ (○) and $CaVO_3$ (⋆) phases.

structural symmetry in the tetragonal form with $a = b = 5.393$ Å and $c = 37.112$ Å matched values previously obtained by other research groups [31, 32].

Substitution of even a small account of V ($\delta = 0.2$) produced the formation of different phases. The BSCCO 2223 phase was perfectly reversed to the $Bi_{1.77}V_{0.15}Sr_{1.97}Ca_{1.13}Cu_{2.07}O_{8+x}$ (nearly BSCCO 2212) phase, but interestingly the orientation on the c axis remained unchanged. Together with this transformation, small amounts of solid solution phases for $SrVO_3$ and $CaVO_3$ were observed (figure 1(b)). The calculated structural parameters for the main phase ($Bi_{1.77}V_{0.15}Sr_{1.97}Ca_{1.13}Cu_{2.07}O_{8+x}$) have a tetragonal symmetry, slightly increased a and b dimensions and significantly decreased c-axis parameter ($a = b = 5.413$ Å and $c = 30.701$ Å), with respect to $\delta = 0$; these parameters were found to be close to the BSCCO 2212 phase ($a = b = 5.39$ Å and $c = 30.601$ Å) [31, 33, 34]. This suggests that the V ions are introduced into the structure of the BSCCO system and this them results in a change in the unit-cell parameters.

When substitution of V increased to $\delta = 0.4$ (figure 1(c)), increased amounts of $SrVO_3$ and $CaVO_3$ impurity solid solution phases were formed. A slight change was also obtained in the main XRD pattern of the system with respect to $\delta = 0.2$. This further suggests that the ionic diffusion of V ions are activated by increasing the V concentration. In conjunction with the SEM–EDXA, the main phase was found to be $Bi_{1.7}V_{0.31}Sr_{1.96}Ca_{1.11}Cu_{2.05}O_{8+x}$; this is also close to the BSCCO 2212 phase. In this case, the tetragonal symmetry of the main phase has unit-cell constants $a = b = 5.4461$ Å and $c = 30.0182$ Å, indicating the continuity of decrease in the c-axis parameter and slight increases in the a-axis and b-axis parameters which compares with previous compositions.

A structural transformation from tetragonal to orthorhombic form was observed when substitution of V increased to $\delta = 0.6$. The main peaks of the $Bi_{1.77}V_{0.15}Sr_{1.97}Ca_{1.13}Cu_{2.07}O_{8+x}$ and $Bi_{1.7}V_{0.31}Sr_{1.96}Ca_{1.11}Cu_{2.05}O_{8+x}$ phases completely disappeared, and the impurity phases of $SrVO_3$ and $CaVO_3$ were also decreased (figure 1(d)). The resultant new material was found to be single-phase $Bi_{1.57}V_{0.48}Sr_{1.94}Ca_{1.10}Cu_{2.00}O_{8+x}$, orthorhombic in structural symmetry with unit-cell constants $a = 5.99$ Å, $b = 5.476$ Å and $c = 29.871$ Å. This phase formation is believed to be a result of the new formation in the Bi–O double layers; this, in turn, would affect the other slabs of $SrO/CuO_2/CaO/CuO_2/SrO$.

On the other hand, a further increase in V content to $\delta = 0.8$ produced a complex structure (figure 1(e). In particular, solid solution phases of $SrVO_3$, $CaVO_3$ and BSCCO 2201 were developed together with the $Bi_{1.31}V_{0.54}Sr_{1.85}Ca_{0.92}Cu_{1.96}O_{8+y}$ main phase. The slightly shifted and high-intensity peaks of the main phase resulted in orthorhombic symmetry with lattice constants $a = 6.215$ Å, $b = 5.490$ Å and $c = 28.437$ Å.

No significant change in the phase formation exists when the V concentration is increased to $\delta = 1.0$. Similar impurity matrices and structural symmetry were obtained as in the $\delta = 0.8$ compound, but very little change in the unit-cell parameters was found: $a = 6.219$ Å, $b = 5.495$ Å and $c = 28.432$ Å.

In general, completely single-phase structures were obtained for $\delta = 0$ and $\delta = 0.6$, but a few solid solution impurity phases have been observed for $0.2 \leqslant \delta < 0.6$. However, in the case when $\delta > 0.6$, the structure was completely deformed; complex and multiphase matrices were obtained. This suggests that the solid solubility of V in the BSCCO 2223 system is limited. At lower concentrations of V ions ($\delta < 0.6$), the XRD peaks have been indexed on the basis of a tetragonal structure but, when the V concentration is increased to $\delta \geqslant 0.6$, a tetragonal-to-orthorhombic phase transformation was obtained. An increase in the a-axis parameter exists if the V concentration is increased. In contrast with the a-axis parameter increase, the c-axis parameter decreases, but the b-axis parameter remains almost unchanged (figure 2). This is to be expected, because the ionic radius of Bi^{3+}($r = 0.96$ Å) is always greater that of V ($r = 0.88$ Å for V^{2+}, $r = 0.74$ Å for V^{3+}, $r = 0.63$ Å for V^{4+} and $r = 0.59$ Å for V^{5+}). It is well known that the cation state of Bi is 3+ [13, 14, 35]. However, it is quite difficult to obtain precise information about the cation state of V ions owing to the extremely unstable electronic nature of this element in this kind of multi-component oxide system. However, the expectation here was that the V ions are in a higher cation state (at least 3+ or higher), because introducing extra electrons by increasing the V concentration may produce a reduced effective valence state on the other elements. For instance, if it is effective on Cu (which is highly possible), it then results in an increase in the Cu–O bonding length; so this could increase the a-axis parameter.

It is believed that the decrease in the c-axis parameter is also related to the excess oxygen in the Bi–O layers, because an increase in the V-ion concentration increases the oxygen content, particularly in the Bi–O layer. This means that the negative charge distribution

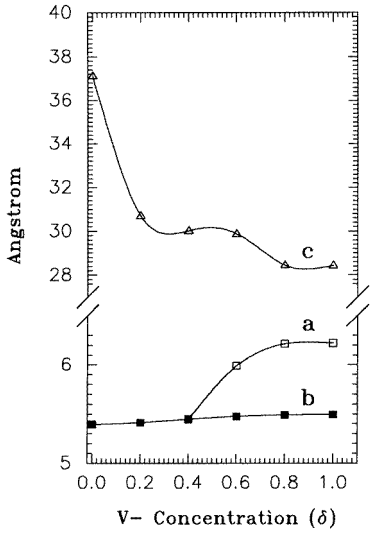

Figure 2. Metamorphosis of unit cell parameters depending on the V concentration δ.

can be altered by extra positive charges and hence repulsion between the layers decreases; so it may cause shrinkage on SrO/BiO/BiO/SrO slabs, which then results in a decrease in the *c*-axis parameter as suggested in the case of doping rare earths into the YBCO system [36, 37].

3.2. Scanning electron microscopy–energy dispersive x-ray analysis

A microanalysis of the V-containing phases and morphology of the samples has been performed by SEM and EDXA. The microstructures of the samples for $\delta = 0$, 0.4 and 0.8 after annealing are shown in figures 3(a), 3(b) and 3(c), respectively.

The $\delta = 0$ sample consisted of fully single-phase BSCCO 2223 (figure 3(a)). The microqualitative analysis showed that this material was compositionally in the $Bi_{1.98}Sr_{1.99}Ca_{1.92}Cu_{2.96}O_{10+y}$ form (the error is less than 2%). It must be noted that the cracks and small holes which appeared as a dark zone occurred during the etching and polishing stages and do not represent individual phases.

In the case of the $\delta = 0.4$ sample, the morphology of the sample was found to be different from that of the $\delta = 0$ sample (figure 3(b)). According to microqualitative analysis, the sample consists mainly of the crystalline phase $Bi_{1.7}V_{0.31}Sr_{1.96}Ca_{1.11}Cu_{2.05}O_{8+y}$ and this phase was surrounded by the $SrVO_3$ and/or $CaVO_3$ solid solution phases. A very small amount of CuO was also detected.

On the contrary, the morphology of the $\delta = 0.8$ sample was found to be more complex than that of the $\delta = 0.4$ sample. The randomly oriented crystals are composed of $SrVO_3$, $CaVO_3$, $Bi_{1.96}Sr_{1.99}Cu_{1.03}O_{6+y}$ and $Bi_{1.31}V_{0.59}Sr_{1.85}Ca_{0.92}Cu_{1.96}O_{8+y}$ (figure 3(c)). In particular, there was found to be more $SrVO_3$ phase in this material. This indicates that the amount of $SrVO_3$ phase increases when the V content in the initial material increases. Interestingly, in the BSCCO system, the frequently obtained solid solution matrices of $(CaSr)_xO_y$ and $(CaSr)_xCu_yO_z$ [35] were not grown in the V-substituted materials. This would suggest that the nucleation and growth of these particular phases could not be favoured

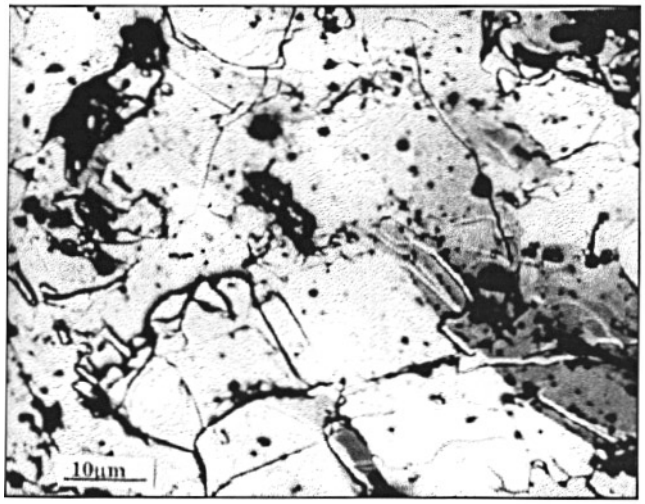

(a)

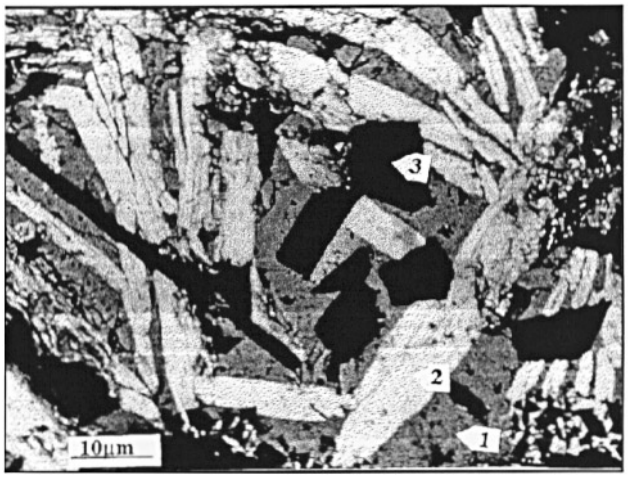

(b)

Figure 3. Scanning electron micrographs of samples. (a) For $\delta = 0$, the single-crystal phase was found to be $Bi_{1.31}Sr_{1.99}$ $Ca_{1.92}Cu_{2.96}O_{10+y}$. (b) For $\delta = 0.4$, crystalline phases are indicated as follows: 1, $Bi_{1.7}V_{0.31}Sr_{1.96}Ca_{1.11}Cu_{2.05}O_{8+y}$; 2, $SrVO_3$; 3, $CaVO_3$. (c) For $\delta = 0.8$, crystalline phases are indicated as follows: 1, $Bi_{1.96}Sr_{1.99}Cu_{1.03}O_{6+y}$; 2, $Bi_{1.31}V_{0.54}Sr_{1.85}Ca_{0.92}$ $Cu_{1.96}O_{8+y}$; 3, $SrVO_3$; 4,$CaVO_3$.

in the case of V substitution. Instead of this, the growth of the $SrVO_3$ and $CaVO_3$ phases was found to be much easier and related well to the solubility of the V ions.

3.3. Fourier transform infrared analysis

Optical phonons and their interactions with other elementary excitations in high-temperature superconductors is quite interesting. By using IR spectroscopy, identification of the excitations responsible for the pairing mechanism was possible.

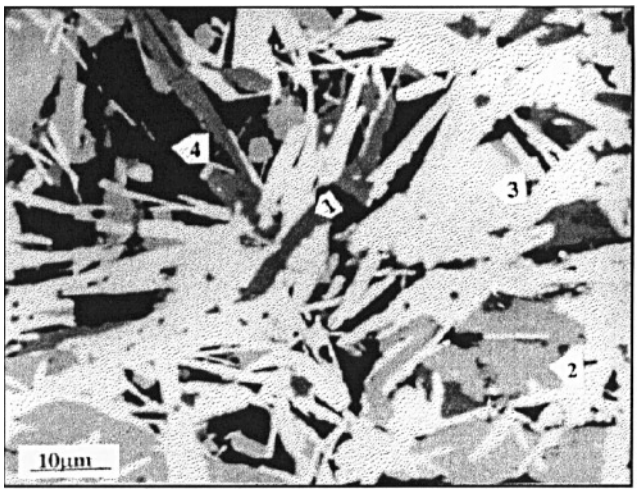

(c)

Figure 3. (Continued)

The IR spectra of materials are shown in figure 4 and the phonon peaks visible at 300 K are listed in table 2. As seen in figure 4, the absorbance spectra of the materials can easily be separated into two regions. The first region consisted of 400–650 cm^{-1} and the second region consisted of 650–1000 cm^{-1}.

Table 2. IR bands obtained for the $Bi_{2-\delta}V_\delta Sr_2Ca_2Cu_3O_{10+y}$ system.

IR bands (cm^{-1})							
$\delta = 0.0$	$\delta = 0.2$	$\delta = 0.4$	$\delta = 0.6$	$\delta = 0.8$	$\delta = 1.0$	$SrVO_3$	$CaVO_3$
409	410	410	411	413	415	497	420
431	435	435	437	438	438	505	455
445	530	533	536	537	537	590	577
455	599	599	603	604	607	830	799
474	737	739	740	740	740	954	909
510	799	799	800	800	800	—	—
542	814	815	815	815	815	—	—
556	866	869	870	871	870	—	—
570	—	—	—	—	—	—	—
603	—	—	—	—	—	—	—
678	—	—	—	—	—	—	—
707	—	—	—	—	—	—	—

Considering both regions together, the integrated baseline corrected bands of V-substituted materials have been found to be different from the typical behaviour of the BSCCO 2223 system [38]. This rules out possible substitution of V ions into the BSCCO system. The first region from 400 to 650 cm^{-1} contains IR-active phonons of Bi–O, Cu–O_2 and Bi–O–Cu–O vibrations [38] and the broad peak at around 600 cm^{-1} is caused by the characteristic IR-active phonons of the pronounced structure of the BSCCO 2223 phase. However, the visible change observed indicates that the phonons around 600 cm^{-1} soften if the V concentration is increased. It is believed that the carrier concentration is an important

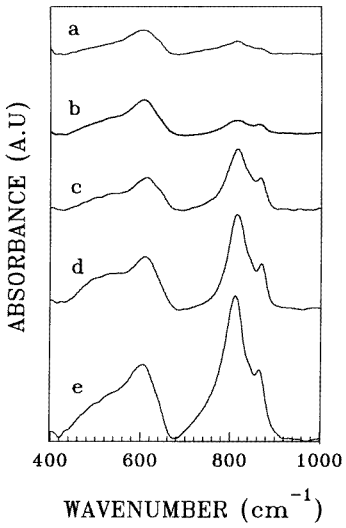

Figure 4. IR spectra of V-substituted materials: curve a, for $\delta = 0.2$; curve b, for $\delta = 0.4$; curve c, for $\delta = 0.6$; curve d, for $\delta = 0.8$; curve e, for $\delta = 1.0$

factor here and, if the carrier concentration is altered on the Cu–O_2 planes by the cation substitution (which produces a change in the Cu–O_2 bonding length, and this could have an effect on the vibration modes), the magnitude and onset point of softening change. the change in the softening point may also be related to the structural transformation obtained in the XRD analysis.

In contrast, in the second region, which extends to high frequencies (650–1000 cm^{-1}) there is a steady increase in absorption. A major change in the phonon structure increasing the V content is clearly visible. This is believed to be a result of the correlation in Bi^{3+}–O/V^{5+}–O vibrations and the amount of the carrier concentration for higher-V-substitution cases. However, this kind of change can also account for the oxygenation effect as suggested for the other families of the high-T_c superconductors [38, 39], because the carrier concentration in the planes of the system can easily be altered by the effect of oxygenation. Together with this consideration, splitting of the prominent band at 800 cm^{-1} when the V concentration is increased may also be a consequence of the structural change in the system as is clearly observed in the XRD analysis, because structural change produces a different bonding distance, and thus different vibration modes. Therefore, one can suggest that the growing bands here could be characterized as IR-active phonon modes of $V^{3+/5+}$–O/$Bi^{3+/5+}$–O (Bi–O–V–O) bonding in the V-substituted system.

3.4. Electrical properties

The electrical properties of the material prepared were examined by resistivity measurements. For the resistivity measurements, well defined metallic behaviour and superconducting transitions are clearly obtained for all compositions except the higher V concentration ($\delta = 0.8$ and $\delta = 1.0$) cases.

As shown in figure 5, curve a, BSCCO 2223 has a metallic behaviour from room temperature to the T_c-value. The critical temperature T_c was found to be 114 ± 0.2 K and the zero-resistance state was found to be at $T_{zero} = 108 \pm 0.2$ K. The DC susceptibility of

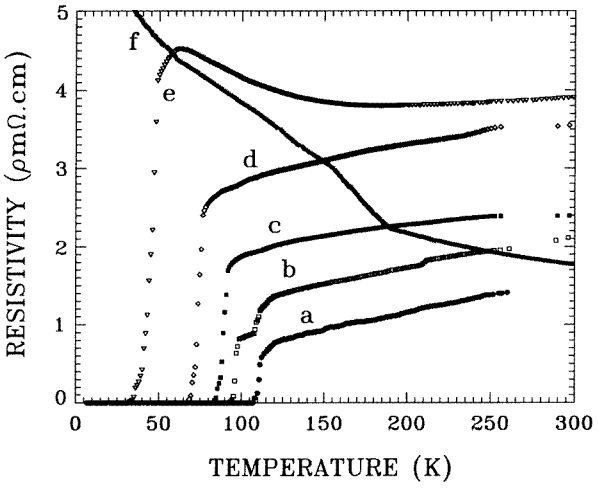

Figure 5. Resistivity measurement result of samples: curve a, for $\delta = 0.0$; curve b, for $\delta = 0.2$; curve c, for $\delta = 0.4$; curve d, for $\delta = 0.6$; curve e, for $\delta = 0.8$; curve f, for $\delta = 1.0$

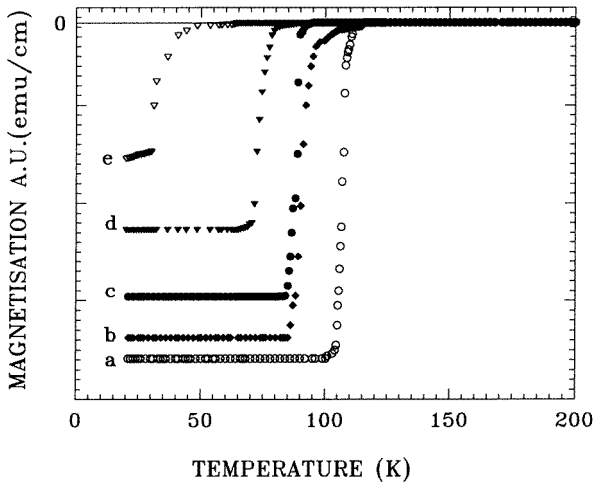

Figure 6. DC susceptibility measurement result of samples: curve a, for $\delta = 0.0$; curve b, for $\delta = 0.2$; curve c, for $\delta = 0.4$; curve d, for $\delta = 0.6$; curve e, for $\delta = 0.8$

the same material also indicates a sharp drop at 114 K (figure 6, curve a). Both results strongly suggest that the structure of this material has a single superconducting phase and supports the XRD and SEM-EDXA results.

However, a change in electrical behaviour has been observed when V substitution is started. As seen in figure 5, curve b, for $\delta = 0.2$, three step transitions have been obtained. The 112 and 97 K transitions indicated that the structure of this material contains a mixed phase of BSCCO 2223 and $Bi_{1.7}V_{0.31}Sr_{1.96}Ca_{1.11}Cu_{2.05}O_{8+y}$, but the $Bi_{1.7}V_{0.31}Sr_{1.96}Ca_{1.11}Cu_{2.05}O_{8+y}$ is dominant in the material since the fraction of the BSCCO 2223 phase is small. The third and relatively small transition at around 210 K

was not reproducible and none of the other samples showed a similar behaviour; also there exists no proof in the magnetization curve of the DC susceptibility measurements (figure 6, curve b). This suggests a filament structure, which is then destroyed by the charge carriers.

When the V concentration is increased to $\delta = 0.4$, the electrical properties decreased further. The material was found to be still metallic up to T_c, but the slope changed slightly compared with the $\delta = 0.2$ case, T_c was found to be 92 K and the gap ΔT between T_c and T_{zero} widens (figure 5, curve c, and table 1).

In the case of the $\delta = 0.6$ sample T_c was found to be 78 K, and then the zero-resistance state was reached at 67 K. The ΔT was also found to be much larger than at the lower substitution levels (figure 5, curve d, and table 1).

For $\delta = 0.8$, semiconducting behaviour was obtained in the temperature region 60–300 K; superconducting behaviour started after 60 K. The T_{zero}-value was reached at around 30 K (figure 5, curve e). For $\delta = 1.0$, semiconducting behaviour continued down to 15 K and then it starts to drop, but it does not reach zero-resistance state (figure 5, curve f). This is as expected, since the impurity solid solution phases of the non-superconductor $SrVO_3$ and $CaVO_3$ and the 10 K superconductor BSCCO 2201 phases were grown together within the $Bi_{1.27}V_{0.69}Sr_{1.80}Ca_{0.88}Cu_{1.90}O_{8+x}$ phase, and this is believed to be responsible for such a dramatic decrease in the superconducting properties.

In general, it is proposed that the superconducting state is destroyed by increasing the V concentration in the BSCCO 2223 system, because the phase coherence of the main BSCCO 2223 structure may in some way be destroyed. It is also believed that the intergrowth of impurity solid solution phase as indicated by the SEM and XRD data and the formation of weak coupling between the larger grains plays a crucial role in diminishing the superconductivity.

The electrical behaviour of the samples also showed strong dependence on the oxygen stoichiometry. For instance, the T_c-values of the quenched materials are comparably lower than for both the oxygen- and the air-annealed samples (table 1). Since the quenching process reduces the oxygen stoichiometry in the BSCCO material, hence it plays a crucial role between the Bi–O double layers.

3.5. Magnetic properties

The susceptibility measurements of the samples showed a paramagnetic behaviour down to the transition temperature. Further cooling to the superconducting state produced a diamagnetic onset for each specimen except for the $\delta = 1.0$ sample.

A sharp drop in the magnetization curve at T_c was obtained for $\delta = 0$; this obviously indicates a good diamagnetic property and superconducting nature due to the formation of the strongly connected grains and growth of the single phase in this specimen (figure 6, curve a).

Increasing the substitution of V produces a visible decrease in the diamagnetic onset temperature of the samples. As seen in figure 6, curve b, in the two-step diamagnetic properties observed for $\delta = 0.2$, the first drop at about 112 K indicates the existence of a small volume fraction of weakly connected grains of the BSCCO 2223 phase, and then a much sharper second step at 97 K implies the second phase, which dominates the rest of the specimen and can be attributed to the bulk superconductor nature of the materials.

In the case of the higher V concentrations, the diamagnetic onset temperatures were observed at 92 K and 78 K for $\delta = 0.4$ and $\delta = 0.6$, respectively (figure 6, curves c and d). For $\delta = 0.8$, the diamagnetic onset was observed at 58 K (figure 6, curve e), but for $\delta = 1.0$ no diamagnetic onset was observed close to 4.5 K, indicating a non-superconducting phase

formation. The sharp drop in the diamagnetic part of the susceptibility pattern at lower concentrations of V can be attributed to the bulk superconductor nature of materials and the strongly connected superconductor grains. A visible widening on the diamagnetic tails at higher substitution levels could be due to the randomly distributed and weakly coupled grains which are responsible for a reduction in the volume fraction of superconductivity in the materials.

For the J_c measurements, the hysteresis cycles were performed at different temperatures for the $\delta = 0.0$, 0.2, 0.4, 0.6 and 0.8 samples; the $\delta = 1.0$ sample was not examined owing to its paramagnetic-like behaviour even in the low-temperature region. The J_c-values of the samples were then determined using Bean's [40] model [41]:

$$J_m = 20\Delta M/a(1 - a/3b) \tag{1}$$

where J_m is the magnetization current density in amperes per square centimetre, $\Delta M = M_+ - M_-$ is measured in electromagnetic units per cubic centimetre, and a and b ($a < b$) are the dimensions in centimetres of the cross section of the sample perpendicular to the applied field.

Figures 7(a) and 7(b) show the typical magnetic hysteresis (M–H) loops of the $\delta = 0.0$ and $\delta = 0.4$ samples, respectively, at four different temperatures. All samples except those with the highest V concentrations showed similar behaviours. In particular for the $\delta = 0.8$ sample, an anomalous magnetization behaviour was found. This is expected owing to the weak superconducting behaviour of these particular samples. However, in the case of the other substitutions, the magnetization decreases when the temperature increases, as expected. These samples also exhibit a field-independent nature after $\mu_0 H > 2$ T for both M_+ and M_- (figures 7(a) and 7(b)).

Figure 8 shows the calculated critical current densities of the samples at a fixed temperature as a function of the applied field. The maximum value of J_c (1.38×10^5 A cm^{-2}) was obtained at 4.5 K for the $\delta = 0$ sample and then decreased when substitution of V increased (table 1). The data obtained at 4.5 K and 15 K indicated the same field dependence of J_c for all samples. However, the values obtained at 25 and 45 K showed weaker field dependence of J_c compared with the values obtained at $T = 4.5$ and 15 K (figure 8). On the other hand, the temperature dependence of the critical current density demonstrates a slight depression on increasing the temperature (figure 9). This kind of behaviour can be explained in terms of an increased volume fraction of non-superconducting grains due to the presence of the V-rich phases.

For all the samples at $T > 15$ K, while a weak magnetic field dependence was still observed, higher values of J_c have been calculated. This is expected because the magnetization curve of the samples forms a loop which indicates the presence of the pinning centres. It is well known that, in high-T_c superconductor materials, non-superconducting impurity phases are highly effective in the flux-pinning mechanism [15, 42]. Thus a higher critical current density together with the small amount of non-superconducting phases is possible.

It can be concluded that the V substitution seems to have an essential influence on the field and temperature dependences of both hysteresis magnetization and the critical current densities for each sample. In contrast with some other elements which were substituted or doped for various compositions of BSCCO and YBCO high-T_c ceramic materials [37, 43], substitution of V does not cause any enhancement of critical current densities in the BSCCO 2223 system.

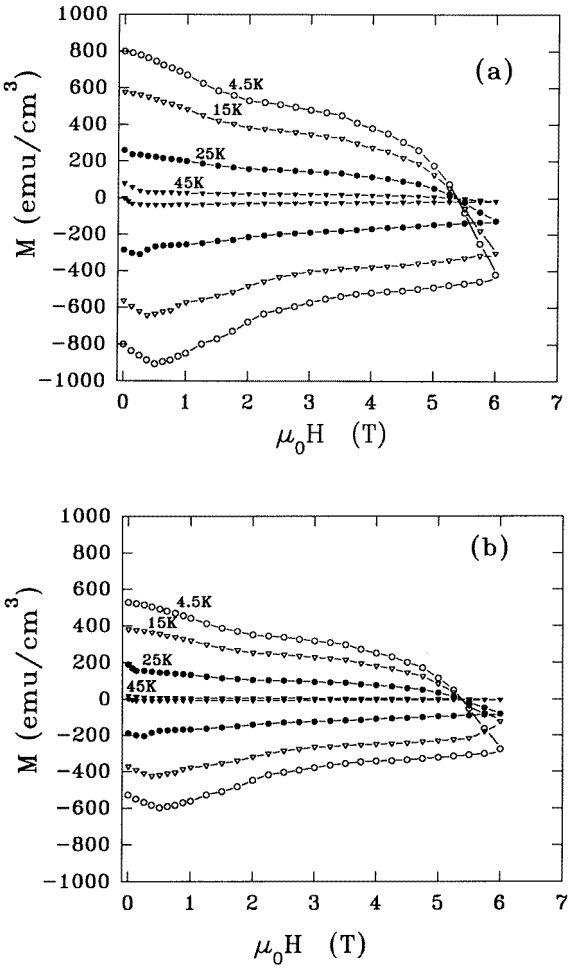

Figure 7. Typical magnetic hysteresis curve of samples: (a) for $\delta = 0.0$; (b) for $\delta = 0.4$.

3.6. Thermal conductivity κ

Thermal conductivity measurements are useful in determining the thermal energy that is transported by charge carriers and phonons. It can provide helpful information about the electron–phonon interaction and other physical properties such as the carrier density and mean free path. Some thermal conductivity measurement data have already been reported for La–Sr–Cu–O [44], Y–Ba–Cu–O [45, 46] and Bi–Pb–Sr–Ca–Cu–O [30]. However, the results obtained show that, in the metallic state ($T > T_c$), the thermal conductivity of high-T_c superconductors is weakly temperature dependent. Although just below the metallic-to-superconducting transition temperature, an increase with a broad peak can be obtained, but in the lower-temperature regions it drops slowly. This rapid rise in κ just below T_c is found to be a unique feature for high-T_c superconductors and is believed to be evidence of an electron–phonon interaction in the structure [30, 44–46].

In this part of the work, the $\delta = 0.2$, 0.4 and 0.6 V-substituted materials and also the $\delta = 0$ materials were investigated owing to their fairly good superconductor properties

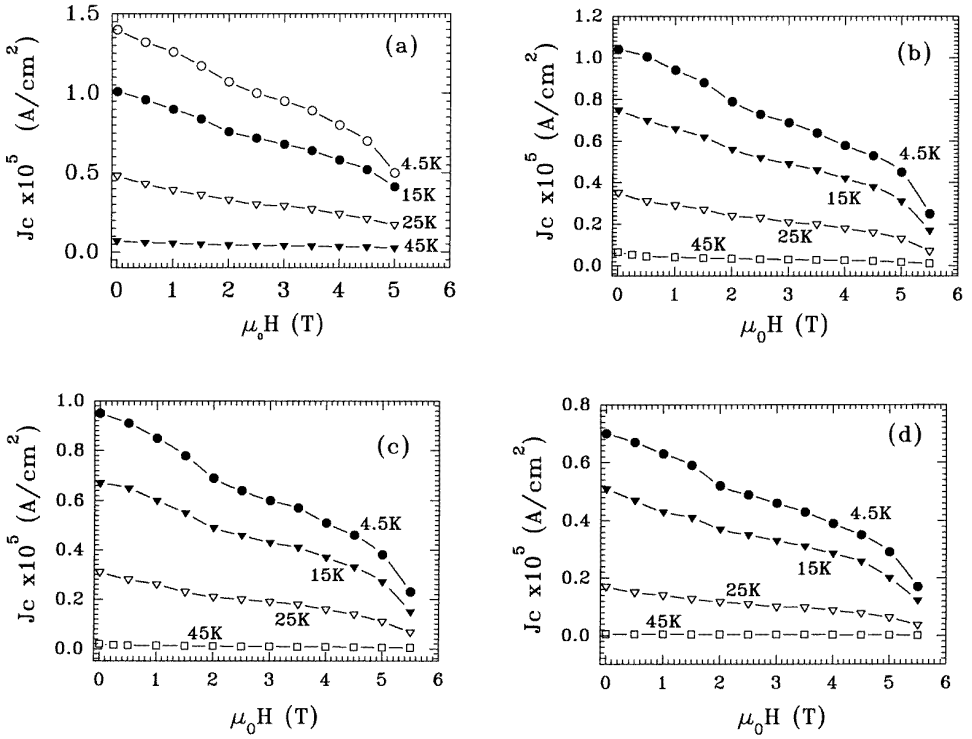

Figure 8. Critical current density versus magnetic field at different temperatures: (a) for $\delta = 0.0$; (b) for $\delta = 0.2$; (c) for $\delta = 0.4$; (d) for $\delta = 0.6$.

compared with the $\delta = 0.8$ and 1.0 materials. The Wiedemann–Franz (WF) law [47], and the measured value of σ were used for all calculations. According to the WF law, the thermal conductivity $\kappa(T)$ can be defined as:

$$\kappa = \pi^2/3(k_B/e)^2\sigma T \equiv L\sigma T. \tag{2}$$

The Lorentz number L is defined as

$$L = \pi^2/3(k_B/e)^2 = 2.45 \times 10^{-8}. \tag{3}$$

By introducing the Lorentz number L into the WF law (equation (2)), the thermal conductivity in different temperature regions (30 K $\leqslant T \leqslant$ 200 K) has been calculated.

As seen in figure 10, the temperature dependence of κ has been observed as linear up to T_c for all samples. At around T_c, a significant rise with a broad maximum and then a sharp drop to the lower-temperature region has been obtained as a characteristic of κ for most metal structures [47–49]. A rise in κ at T_c is believed to be related to the electron–phonon scattering mechanism. Scattering is believed to decrease at this temperature and the mean free path to increase; this produces a freer phonon flow and suggests strong electron–phonon coupling. κ was found to depend on the V concentration; when the V concentration was increased, the thermal conductivity of the material decreased systematically (figure 10). This suggests that the scattering of the electron–phonon couples increased and the mean free path decreased in the BSCCO system with higher concentrations of V.

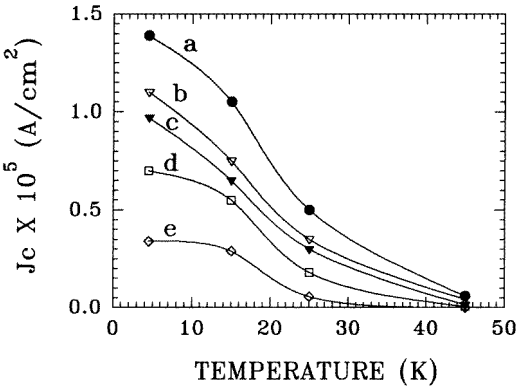

Figure 9. Temperature dependence of J_c: curve a, for $\delta = 0.0$; curve b, for $\delta = 0.2$; curve c, for $\delta = 0.4$; curve d, for $\delta = 0.6$; curve e, for $\delta = 0.8$;

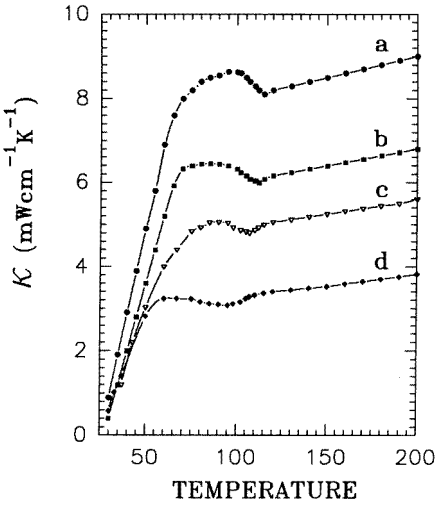

Figure 10. Temperature dependence of thermal conductivity κ: curve a, for $\delta = 0.0$; curve b, for $\delta = 0.2$; curve c, for $\delta = 0.4$; curve d, for $\delta = 0.6$.

4. Conclusion

Structural evolution, electrical resistivity, magnetic properties, current density and thermal conductivity studies were systematically carried out on the $Bi_{2-\delta}V_\delta Sr_2Ca_2Cu_3O_{10+y}$ superconducting system by preparing more than 65 samples. XRD and SEM-EDXA observations indicate a structural transformation and a solubility limit for V ions in the BSCCO 2223 system. In particular, at higher concentrations of V ions, the formation of phases with high V contents were observed. Some of these phases were found not to be constituted by solid solutions of the (Bi–V)–Sr–Ca–Cu–O complex oxide phase; however, such phases grow more rapidly as independent ceramic matrices.

The IR properties of V-substituted materials were found to be different from those of the BSCCO 2223 system. This confirms that a new structural formation which had different

active phonon modes and which suggests a change in the bond distances occurred in the material.

Electrical, magnetic and current density results showed a systematic decrease when the V concentration increases. The weaker magnetic field dependence of J_c is believed to be a consequence of strong pinning in the materials.

The results obtained from the thermal conductivity and also magnetization measurements suggested a strong electron–phonon coupling mechanism. However, the rate of mechanism is largely dependent on the substituent ion concentration.

Acknowledgments

This research was supported by the İnönü University Research Fund under contracts IÜAF-94/17 and 94/18. The author wishes to thank Professor M J Clark, Dr G A Morthaza, Dr İ Aksoy and Dr B Uluğ for their help and for meaningful discussions during this investigation.

References

[1] Maeda H, Tanaka Y, Fukutumi M and Asano T 1988 *Japan. J. Appl. Phys.* **27** L209
[2] Gao L, Huang Z J, Meng R L, Hor P H, Bechtold J, Sun Y Y, Chu C W, Sheng Z Z and Herman A M 1988 *Nature* **332** 623
[3] Chu C W, Bechtold J, Gao L, Hor P H, Huang Z J, Meng R L, Sun Y Y, Wang Q Y and Zue Y Y 1988 *Phys. Rev. Lett.* **60** 941
[4] Tallon J L, Buckley R G, Gilbert P W, Presland M R, Brown I W M, Bowder M E, Christian L A and Gafull R 1988 *Nature* **333** 153
[5] Ramesh R, Hedge M S, Chang C C and Tarascon J M 1989 *J. Appl. Phys.* **66** 4879
[6] Sunshine S, Cava R J, Schneemeyer L F, Murphy P W, Glarum S A, Nakahara S, Rupp L W and Peck W F 1988 *Phys. Rev.* B **38** 893
[7] Kijima N, Gronsky R, Endo H and Ogury Y 1991 *J. Appl. Phys. Lett.* **58** 188
[8] Sakazaki I, Morii K and Nakayama U 1991 *J. Mater. Sci. Lett.* **11** 321
[9] YakıncıM E, Holland D and Blunt L 1991 *Br. Ceram. Proc.* **48** 461
[10] Koyama K, Kamo T and Matsuta S 1990 *Japan. J. Appl. Phys.* **29** L53
[11] Jayaram B, Lanchester P C and Weller M T 1989 *Physica* C **160** 17
[12] Mune P, Altshuler E, Musa J, Garcia S and Riera R 1994 *Physica* C **226** 12
[13] Xiao H G, Xiao G W, Jie L and Gao S 1994 *Phys. Rev.* B **50** 1237
[14] Sumana P P, Rao M S R, Vardaraju U V and Rao G V S 1994 *Phys. Rev.* B **50** 6929
[15] Dimesso L, Matsubara I, Ogura T, Funahashi R, Yamashuta H and Tampieri A 1994 *Physica* C **227** 291
[16] Tanaka K, Nozue A and Kamiya K 1990 *J. Mater. Sci.* **25** 3551
[17] Tsuboi S, Tohge N, Tatsumisagu M and Minami T 1990 *Japan. J. Appl. Phys.* **29** L896
[18] Polonka J, Xu M, Golgman A, Finnemore D K and Li Q 1992 *Supercond. Sci. Technol.* **5** 157
[19] Komatsu T, Sato R, Imai K, Matusita K and Yamashita T 1988 *Japan. J. Appl. Phys.* **27** L1839
[20] Kanai T, Kamo T and Matsuta S 1989 *Japan. J. Appl. Phys.* **28** L2188
[21] Gao Y, Permambuco P W, Crow E J, O'Reilly J, Spencer N, Chen H and Salomon R E 1992 *Phys. Rev.* B **45** 7436
[22] Awana P S V, Agarwal S K, Narlikar A V and Das M P *Phys. Rev.* B **48** 1211
[23] Balkin D and McGinn P 1994 *Supercond. Sci. Technol.* **7** 72
[24] Xin Y, Sheng Z Z, Chan F T, Fung P C W and Wong K W 1990 *Solid State Commun.* **76** 1351
[25] Xin Y, Sheng Z Z, Chan F T, Fung P C W and Wong K W 1990 *Solid State Commun.* **76** 1347
[26] Liu R S, Zhou W, Janes R and Edwards P P 1990 *Solid State Commun.* **76** 1261
[27] Fung P C W, Lin Z C, Liu Z M and Ching W Y 1990 *Solid State Commun.* **75** 211
[28] Fung P C W, Chow J C L and Du Z L 1994 *Supercond. Sci. Technol.* **7** 397
[29] Chanda B and Dey T K 1994 *Solid State Commun.* **89** 353
[30] YakıncıM E, Aksoy I and Ceylan M 1996 *J. Mater Sci.* **31** 2738
[31] Tarascon J M, McKinnon W R, Barbouz P, Greene L H, LePage V and Giroud M 1988 *Phys. Rev.* B **38** 8885

[32] Tallon J L, Buzley R G, Gilbert P W, Presland M R, Brown W M E, Bowden M E, Cristian L A and Goguel R 1988 *Nature* **333** 153
[33] Herviev M, Michel C, Domengues B, Laligant Y, Lebail A, Ferey G and Raveav B 1988 *Mod. Phys. Lett.* B **2** 491
[34] Tarascon J M, LePage V, Barboux P, Bagley B G, Greene L H, McKinnon W R, Hull G W, Giroud M and Hwang D M 1988 *Phys. Rev.* B **37** 9382
[35] YakıncıM E 1992 *PhD Thesis* Department of Physics, University of Warwick, Coventry
[36] Yoo S I, Sakai N, Takaichi H, Higuchi T and Murakami M 1994 *Appl. Phys. Lett.* **65** 633
[37] Xiao Y G, Yin B, Zhao Z X, Ren H T, Xiao L, Fu X K and Xia J A 1994 *Supercond. Sci. Technol.* **7** 623
[38] Uluğ B and YakıncıM E 1994 *Physica* C **235** 1021
[39] Umezawa A, Crabtree G W, Liu J Z and Weber H W 1987 *Phys. Rev.* B **36** 7151
[40] Bean C P 1962 *Phys. Rev. Lett.* **8** 250
[41] Shi D, Boley M S, Welp U, Chen J G and Liao Y 1989 *Phys. Rev.* B **40** 5255
[42] Ogawa N, Yoshida M, Hirabayashi I and Tanaka S 1992 *Supercond. Sci. Technol.* **5** 89
[43] Müller K H and Matthews D N 1993 *Physica* C **206** 275
[44] Bartkowski K, Horyn R, Zaleski A J, Bukowski Z, Horobiowski M, Marucha C, Rafalowicz J, Rogacki K, Stepien D A, Sulkowski C, Trojnar E and Kalamut J 1987 *Solid State Commun.* **63** 973
[45] Gottwick U, Held R, Sparn G, Steglich F, Rietschel H, Ewert D, Renker B, Bauhofer W, Molnar S, Wilhelm M and Hoenig H E 1987 *Europhys Lett.* **4** 1183
[46] Morelli D T, Heremans J and Swets D E 1987 *Phys. Rev.* B **36** 3917
[47] Parrot J E 1975 *Thermal Conductivity of Solids* ed. A D Stuckes (New York: Academic) pp 171–267
[48] Anderson A C 1979 *Fast Ion Transport In Solids* ed P Vashista, J N Mundy and G K Shenoy (Amsterdam: North-Holland) p 225
[49] Anthony P J and Anderson A C 1976 *Phys. Rev.* B **14** 5198